Yuan, K. et al. (2020) '2D Nanomaterials Wrapped Janus Micromotors with Built-in Multiengines for Bubble, Magnetic, and Light Driven Propulsion', Chemistry of materials, 32(5), pp. 1983–1992.

Available at https://doi.org/10.1021/acs.chemmater.9b04873

2D nanomaterials wrapped Janus micromotors with built-in multiengines for bubble, magnetic, and light driven propulsion

Kaisong Yuan,[†§] Víctor de la Asunción-Nadal,[†] Beatriz Jurado Sánchez,[†‡*] Alberto Escarpa[†‡*]

[†]Department of Analytical Chemistry, Physical Chemistry and Chemical Engineering, University of Alcala, Alcala de Henares E-28871, Madrid, Spain. E-mail: beatriz.jurado@uah.es, alberto.escarpa@uah.es (Tel: +34 91 8854995)

[§]Institute of Pharmaceutical Analysis, College of Pharmacy, Jinan University, Guangzhou, China

[‡]Chemical Research Institute "Andrés M. del Río", University of Alcala, Alcala de Henares E-28871, Madrid, Spain

ABSTRACT: Graphene oxide, graphdyine and black-phosphorus coated micromotors integrating *"three engines"* for motion control using different stimuli such as chemical fuel, light and magnetic fields are described. Micromotors can be mass-produced by wrapping gold-sputtered polystyrene microspheres with the 2D nanomaterials, followed by simultaneous assembly of Pt or MnO_2 nanoparticles (NPs) as "*bubble (catalytic)-engines*"; Fe_2O_3 NPs as *"magnetic engines"* and quantum dots (QDs) as *"light engines"*. Micromotors design and composition is key to get the desired propulsion performance. In *bubble-magnetic* and *bubble-light mode*, a *"built-in"* acceleration system allows to increase micromotor speed up to 3.0 and 1.5 times after application of the magnetic field or light irradiation, respectively. In *bubble-magnetic-light* mode, such speed increase can be combined in a single unit for *on-demand* braking and accelerating systems. Fluid dynamics simulations illustrate that such adaptative behavior and improved propulsion efficiency is produced by a better distribution of the fuel and thus energy propelling the micromotor by activation of the *magnetic* and/or *light* engines. The new micromotors described here -which combine multiple engines with functional nanomaterials - hold considerable promise to develop novel nanovehicles with adaptative behavior to perform complex tasks in lab-on-a-chip or dynamic micropatterning applications.

INTRODUCTION

Nano and micromotors can be defined as tools-with a size ranging from few nanometers to micrometers- that can convert a chemical fuel, light, magnetic or acoustic energy input into autonomous motion to perform several tasks.[1-10] Current efforts in the field are aimed to impart them with adaptative moving behaviors to improve overall functionality in complex environments.[11-14] Judicious design of the micromotor structure allows to incorporate different functionalities in a single unit for further control their propulsion behavior and motion direction with different energy sources (one or two stimuli) to speed-up, stop or reverse their navigation. For example, a magnetocatalytic hybrid micromotor reported by Wang´s group consists of an Au-Pt nanowire (responsible for catalytic propulsion) with a Ni tail connected by an Ag segment (for magnetic propulsion). Such early design holds considerable promise to address hampering locomotion of the catalytic/phoretic mode in salt-rich complex media by the application of a magnetic field.[15] Later on, our research group developed Janus micromotors containing Pt/Fe_2O_3 nanoparticles (NPs) for dual magnetic and chemical propulsion. Such dual behavior allows to perform bacteria endotoxin sensing in lab-on-a-chip sensors.[16] Magneto-acoustic hybrid micromotors combine a ferromagnetic Ni-coated Pd helical structures with an ultrasound-active gold concave nanowire end for dual-hybrid behavior in future biomedical applications where the magnetic behavior can assist to reach hard to access areas (*i.e.* hard tissues).[17] Catalytic-acoustic hybrid schemes allow to stop-control micromotor motion and to induce a swarming behavior for future cargo capture and transport; with designs relying on Au-Ru[18] or Au-Pt nanowires[19] and even PEDOT/Ni/Pt[20] tubular micromotors whose motion can be stopped by hindering bubble ejection under ultrasound fields. Au/Ru core–shell nanowires motors can propel by a combination of self-diffusiophoresis and electroosmosis forces in peroxide solutions by simply tailoring its length.[21] Recently, the convenient marriage between light and catalytic, magnetic or ultrasound propulsion has led to the design of micromotors with *"built-in"* braking and accelerating systems for future motion control and improved performance.[22-25] Thus, the autonomous motion of light-sensitive TiO_2/Au/Pt Janus micromotors in hydrogen peroxide solutions can be reversed by ultraviolet (UV) light irradiation by changing the "active" catalyst site from Pt to TiO_2.[26] The different catalytic activities of both metals result in such braking/acceleration behavior. Black TiO_2/Au Janus micromotors display a multiwavelength light-responsive behavior for autonomous propulsion both in H_2O_2 solutions and in water over a broad range of wavelengths (UV, blue, cyan, green, and red light).[27] Similarly, our group described the acceleration of multi-light driven quantum dots sensitized fullerene based tubular micromotors with Pt, Pd or MnO_2 as inner catalytic layers. Upon light irradiation (from 385 to 670 nm), electrons released from the CdS QDs are trapped in the catalytic layers, resulting in a negative net charge in the metal side, which reacts with oxygen and protons present in the media, generating additional H_2O_2 or O_2 input, which is further decomposed and increases the overall micromotor speed.[28] ZnO/Pt tubular micromotors display a similar *"on-the-fly"* optical acceleration nature.[29] Interestingly, the incorporation of a Ni layer into such ZnO based tubular micromotors introduce additional *magnetic-light* controlled propulsion capabilities.[13]

Apart from the inherent adaptative motion capabilities, a key to develop micromotors with high performance for future applications is to explore the incorporation of advanced functional materials for further functionalization. In addition, carbon nanomaterials,[30-34] black phosphorous,[35] molybdenum disulfide

(MoS_2)[36] or tungsten disulfide (WS_2)[37] impart the micromotors with a rough surface area for the subsequent incorporation of a higher loading of the active nanoparticles, which are responsible for the motion control behavior, allowing thus to tune the propulsion mode. For example, Pumera's group illustrates that the motion of mesoporous ZnO/Pt Janus depends on the surface roughness, with a pure diffusiophoretic motion for rough micromotors and fuel-free UV light propulsion for smooth micromotors.[38] Yet, the incorporation of functional nanomaterials into micromotors units and the influence in the motion control behavior remains unexplored to date. In addition, only dual stimulates have been described (*magnetic-catalytic*, *magnetic-acoustic*, *catalytic-acoustic*, *magnetic-light* and *acoustic-light*), without attempts to incorporate additional modes (triple or more stimulates) for forthcoming applications.

To address the above-mentioned gaps, herein we report the preparation of 2D nanomaterials coated micromotors integrating *"three engines"* for motion control using different stimuli such as chemical fuel, light and magnetic fields. Unlike previous works, here we will study the influence of the micromotor composition in the propulsion modality, which allows adapting its composition *"on-demand"* for a given application in a specific media. Micromotors can be mass-produced by wrapping gold-sputtered polystyrene (PS) microspheres with already explored (graphene oxide, GO) and novel 2D nanomaterials (black phosphorous, BP and graphdyine oxide, GDY). The concept is illustrated in **Figure 1**. As can be seen, Pt or MnO_2 NPs were used as engines for *"bubble (catalytic)-propulsion"*; Fe_2O_3 NPs as *"magnetic mode"* handles and QDs as *"light mode"* engines (see **Figure 1A**). In the following sections, we will characterize each motion modality, study the influence of the 2D nanomaterials, catalyst and peroxide or light intensity upon the propulsion performance as well as by fluid dynamics simulations. Such knowledge will allow for additional control of the micromotor moving behavior for a given application.

EXPERIMENTAL SECTION

Reagents and materials. Polystyrene microparticles (cat. 87896), benzyl alcohol (cat. 305197), thioglycolic acid (cat. T3758), N-(3-Dimethylaminopropyl)-N′-ethylcarbodiimide hydrochloride (cat. 03449), hydrazine solution (cat. 309400), graphene oxide (cat. 763705), black phosphorus (cat. 808970), polyethylenimine (cat. 408727), iron (III) oxide (cat. 544884), chloroplatinic acid hydrate (cat. 398322), hydrogen peroxide (cat. 216763), cysteamine (cat. M9768), potassium permanganate (cat. 223468), CdSe@ZnS alloyed quantum dots kit (cat. 753904) were purchased from Sigma-Aldrich (Spain). Sodium dodecyl sulfate (cat. 71727) was supplied by Merck (Germany). All reagents were used without further purification. Graphdiyne was provided by Li et al, used as received without further purification. The synthesis method has been described in a previous work.[39] An inverted optical microscope (Nikon Eclipse Instrument Inc. TiS/L100), coupled with 20X and 40X objectives, a Zyla cMOS digital camera and NIS Elements AR 3.2 software, was utilized for capturing movies. The speed of the micromotors was tracked using a NIS Elements tracking module. Various filters cubes were used to obtain the different light emissions: DAPI (382-393 nm), FITC (467-498 nm), G-2A (510-560 nm).

Preparation of polystyrene-gold (PS-Au) Janus microparticles. Firstly, ordinary glass slide substrates were washed with acetone, ethanol, and pure water in an ultrasonic bath. Secondly, PS microparticles (aqueous suspension concentration: 2%) were dropped on the clean glass slide to from a monolayer at room temperature. The successful generation was checked by optical microscopy. Thirdly, large-scale PS monolayers would thus be form on the glass slide, and then sputtered with a ~50 nm gold layer. At last, PS-Au monolayers were transferred to the pure water for the further modification.

Synthesis of graphene oxide (GO) coated PS-Au Janus microparticles. For the preparation of sulfhydryl- modified graphene oxide (HS-GO), GO (dispersion in water, 10 mL, 0.1 mg/mL) was first mixed with 0.15 g N-(3-Dimethylaminopropyl)-N′-ethylcarbodiimide hydrochloride (EDC) overnight to fully active the carboxyl groups on the GO surfaces, then 10 mg of cysteamine (Cys) were added and mixed for another 2 h. After that, GO solution was centrifuged at 10,000 rpm for 5 min, washed with ultrapure pure water 3 times to remove the excess of Cys and diluted to 10 mL of ultrapure water for further used. For the preparation of GO coated microparticles, 0.1 mL of the above HS-GO solution was mixed with PS-Au microparticles (0.9 mL) for 2 h to make HS-GO adhere to gold side of the PS-Au. Then the reaction solution was filtered with cyclopore track etched membrane (5 µm) to remove the free HS-GO. Herein, the GO coated PS-Au was obtained.

Synthesis of graphdiyne oxide (GDYO) coated PS-Au Janus microparticles. GDYO were made similar to an acid-oxidation method reported by Qi et al,[40] in which 2 mg of graphdiyne (GDY) was mixed with HNO_3 (0.4 mL), H_2SO_4 (0.6 mL), and $KMnO_4$ (4 mg) and stirred vigorously for 8 h at 100 °C. The reaction solution was cooled to room temperature and the pH was adjusted to 8.0 with NaOH in an ice-bath. Next, the solution was centrifuged at 10,000 rpm for 5 min and washed with ultrapure water 3 times. Herein, the GDYO was obtained. For the preparation of sulfydryl- modified graphdiyne oxide (HS-GDYO), GDYO (dispersion in water, 10 mL, 0.1 mg/mL) was first mixed with 0.15 g EDC overnight, then 10 mg of Cys were added and mixed for another 2 h. After that, GDYO solution was centrifuged at 10000 rpm for 5 min, and washed with pure water for 3 times. All the obtained HS-GDYO was diluted to 10 mL of pure water for further used. At last, same process as the synthesis of GO coated PS-Au were made to further coating the PS-Au with GDYO.

Synthesis of black phosphorus (BP) coated PS-Au Janus microparticles. Two-dimensional BP were made by a previous report with some modification.[41] A home-made setup was prepared for ultrasonic exfoliation of BP crystals. A 2% w/v SDS (20 mL) solution containing 1 mg of BP crystals inside the home-made setup was first purged with ultrahigh purity grade N_2 for 30 min to remove dissolved oxygen. Then the interface between balloon and lip, horn sonication and lip were sealed with Pattex® Nural 21 several times to occlude O_2 from the outside surrounding. BP crystals inside the setup were then exfoliated by ultrasonication at 70 W for 1 h in an ice bath. After that, the solution was washed with pure water for 3 times. For the preparation of sulfydryl- modified black phosphorus (HS-BP), BP (dispersion in water, 5 mL, 0.1 mg/mL) was first mixed with 2 mg of polyethylenimine (PEI) overnight.[42] Then the reaction solution was centrifuged at 10000 rpm for 5 min and washed with pure water 3 times to get the PEI@BP. The obtained PEI@BP was re-dispersed in 5 mL of pure water, then 100 µL of thioglycolic acid (10 mg/mL) were added and mixed for 2 h. After that, the solution was centrifuged at 10,000 rpm for 5 min and washed with pure water 3 times to get the HS-BP. At last, same process as the synthesis of GO and GDY coated PS-Au were made to further coating the PS-Au with BP.

Preparation of Pt or MnO_2 based 2D material-PS Janus micromotors. PtNPs were assembled into the 2D materials surfaces by an in-situ synthesis method.[43] The 2D materials coated PS-Au Janus micromotors were diluted with ultrapure

water (final volume: 1 mL), then 200 µL of chloroplatinic acid hydrate (1 mg/mL) and 20 µL of hydrazine solution (35 wt. % in H_2O) were added and mixed for 2 h. After that, reaction solution was filtered with a cyclopore track etched membrane (5 µm) to remove free PtNPs. Herein, Pt-2D material-PS Janus micromotors were obtained. Fabrication of MnO_2 NPs onto the 2D materials surfaces are conducted by an in-situ synthesis method.[44] The 2D materials coated PS-Au Janus micromotors were diluted with pure water (final volume: 1 mL), then 200 µL of potassium permanganate ($KMnO_4$, 2 mg/mL) and 10 µL of benzyl alcohol (anhydrous, 99.8%) were added and mixed for 5 h. After that, reaction solution was filtered with cyclopore track etched membrane (5 µm) to remove the free MnO_2NPs. Herein, the MnO_2-2D material-PS Janus micromotors were obtained.

Preparation of Pt and MnO_2 based Janus micromotors with magnetic Fe_2O_3 NPs and CdSe@ZnS quantum dots. For the fabrication of Pt or MnO_2 based Janus micromotors with magnetic Fe_2O_3 NPs, 1 mL of Pt or MnO_2 based Janus micromotors were mixed with 20 µL of Fe_2O_3 NPs (1 mg/mL) for 1 h and then filtered with cyclopore track etched membrane (5 µm) to remove the free Fe_2O_3 NPs. Herein, the magnetic Pt based Janus micromotors were obtained. For the fabrication of Pt or MnO_2 based Janus micromotors with magnetic Fe_2O_3 NPs and CdSe@ZnS quantum dots, the above magnetic Pt based Janus micromotors were mixed with 5 µL of CdSe@ZnS quantum dots for 1 h, and then filtered with cyclopore track etched membrane (5 µm) to remove the free quantum dots.

RESULTS AND DISCUSSION

Figure 1 illustrates the concept of the multi-light driven micromotor. In all cases, and as reflected in the time-lapse images and corresponding tracking lines of **Figure 1B**; in *bubble-magnetic* and *bubble-light mode*, the *"built-in"* system allows to increase micromotor propulsion up to 3 and 1.5 times after application of the magnetic fields or light irradiation, respectively. In *bubble-light-magnetic mode*, such speed improvement can be combined for *on-demand* braking and accelerating systems (see speed profiles in **Figure 1C**).

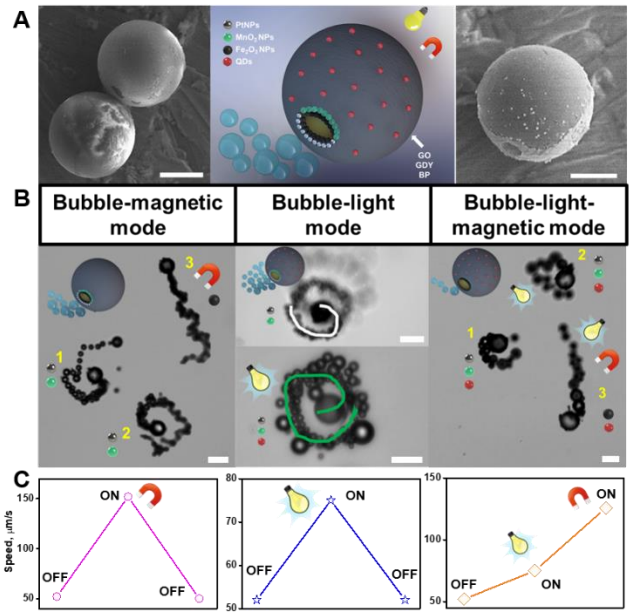

Figure 1. A) Scanning-electron microscopy (SEM) images of the morphology of the micromotors (left and right images) and schematic of the micromotor structure (middle). Gold sputtered PS spheres (20 µm) are wrapped with GO, GDY or BP as nanomaterials and Pt or MnO_2 NPs as engines for *"bubble-propulsion"*; Fe_2O_3 NPs as *"magnetic mode"* engines and CdSe@ZnS QDs as *"light mode"* engine. Scale bars, 10 µm. B) Time-lapse images (taken from **Video S1**) showing the hybrid propulsion modes of a GDY/Pt- Fe_2O_3-QDs Janus micromotors in 5 % hydrogen peroxide solutions and C) corresponding speed profiles. Scale bars, 20 µm.

As reflected in **Figures 1 and 2**, judicious micromotors design is key to get the desired propulsion performance. For Janus particles, the generation of a well-defined asymmetric patch in the structure is essential for the particle to experience a strong anisotropy. This will result in the accumulation of reaction products (from fuel or sample decomposition) in one side of the microparticle for directional propulsion.[45, 46] For the synthesis, we adopt a two-step protocol combining physical vapor deposition and liquid phase deposition (chemical and self-assembly) as shown in **Figure 2A**. First, PS nanoparticles were selected as a scaffold and coated with a thin gold layer (50 nm) which will play a dual role for nanomaterial and catalytic nanoparticles assembly (see experimental section for further details). Prior assembly, GO, GDY or BP were modified by the introduction of sulfhydryl (HS) group via activation of the -COOH functional groups present in the materials (for GO and GDY) or by the introduction of polyethyleneimine groups, as described in the experimental section. Next, Pt or MnO_2 NPs were synthesized *in-situ* in the presence of Au-2D nanomaterials coated microspheres following a seed-mediated growth type mechanism.[47-49] To this end, we optimize the amount of nanomaterial for incubation with the Au-modified PS microspheres in order to get a small exposed gold area to promote such preferential growth. Thus, we incubate a fixed number of Au-PS microspheres with different amounts of 0.1 mg/mL solutions of sulfhydryl modified GO, GDY and BP followed by PtNPs generation. Next, several drops (1 µL) of the as-obtained micromotors were placed on a glass slide under the microscope to check the number of motile micromotors (which was related with the successful incorporation of the PtNPs due to the presence of exposed gold). In all cases, the highest percentage of moving micromotors (80 %) was obtained using 100 µL of the 2D nanomaterials solutions, whereas for higher

volumes/amounts, only 5 % of the micromotors were motile. Finally, Fe_2O_3 and CdSe@ZnS nanoparticles were self-assembled by incubation with the Pt-NPs or MnO_2-NPs. The Janus structure and successful element incorporation in the micromotors are reflected in the SEM and EDX images of **Figure 2B**, which illustrate that the 2D nanomaterials cover the whole micromotor structure, with only a small part (the asymmetric patch) covered with Pt, MnO_2 or Fe_2O_3 NPs. UV-Vis observation reveals the successful incorporation of the CdSe@ZnS QDs due to the appearance of the particular adsorption band; which cannot be observed in bare micromotor solutions (see **Figure 2C**). Additional Raman mapping of the micromotors indicates the presence of the nanomaterials (see **Figure 2D**). For GO and GDY both D-band and G-band are clearly distinguished with minor differences with the characteristic D and G bands of both nanomaterials;[50, 51] whereas for BP the three prominent peaks of the A^1_g (360 cm^{-1}), B_{2g} (440 cm^{-1}) and A^2_g, (466 cm^{-1}) phonon modes are present.[52] Simultaneously, AFM images were taken, illustrating the rough morphology of the GDY coating the micromotors (**Figure 2E**, top) and the characteristic morphology of a BP flake attached to the micromotor surface (**Figure 2E**, bottom).[52]

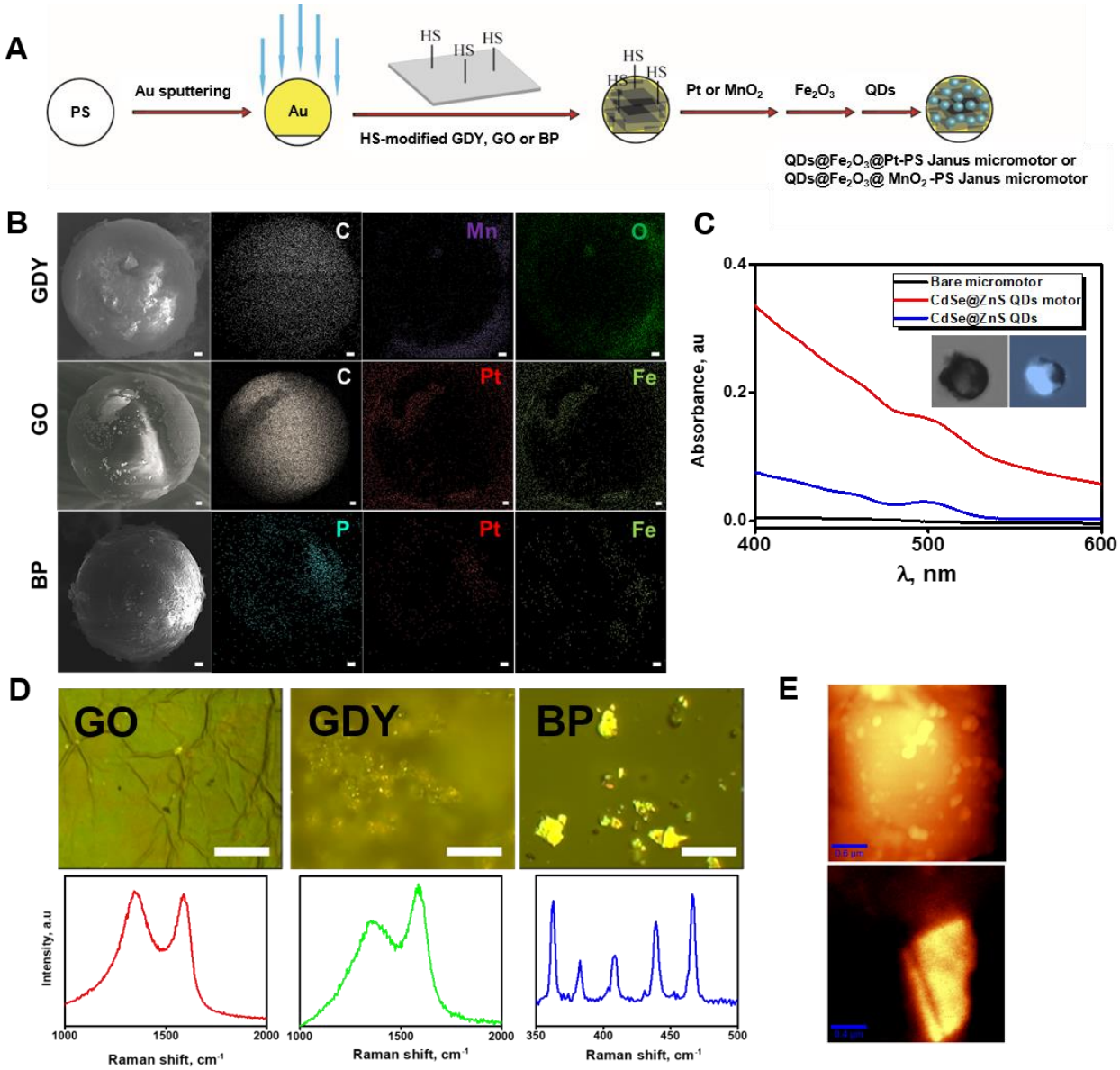

Figure 2. A) Schematic of the Janus micromotor synthesis: 50 nm gold layer sputtered PS nanoparticles are incubated with thiol modified nanomaterials (GO, GDY or BP). After assembly to the nanoparticles surface, Pt or MnO_2 are generated *"in-situ"* in the presence of the Janus micromotors, following Fe_2O_3 and QDs assembly. B) SEM and energy-dispersive X-ray (EDX) characterization of the micromotors and element distribution. Scale bars, 1 µm. C) UV-Vis spectra of CdSe@ZnS QDs, bare and QDs wrapped micromotors. D) Optical microscopy images of a selected area of the micromotors and corresponding Raman spectra.–Scale bars, 10 µm. E) AFM images of GDY and BP over the micromotor surface. Scale bars, 0.6 (top) and 0.4 µm (bottom).

We next evaluated the micromotor propulsion in *bubble-magnetic* mode. The time-lapse images of **Figure 3A** illustrate the propulsion of GO/GDY/BP-QDs-Pt-Fe_2O_3 or GO/GDY/BP-QDs-MnO_2-Fe_2O_3-PS Janus micromotors in 5 % peroxide solutions before (top images) and after application of a magnetic field (bottom). Magnetic field was applied using a permanent

neodymium magnet (N35, intensity 1.1 T). The magnet was placed at a distance of about 20 cm from the micromotor sample. At such distance, the magnetic field is parallel and doesn't exert a towing force on the motor, and it only generates the motor to orientate towards the applied magnetic field. Such magnet can be easily replaced by electromagnets or permanent magnets for future applications beyond the scope of this article. A change in the trajectory from turbulent to directional can be clearly observed by the application of the magnetic field (Fe_2O_3 engine). This cause a change in the flow speed mapping around the Janus micromotors, which result in a speed increase for *braking/acceleration* of the micromotor, which could be very useful for future applications in complex media. Prior to further explaining the phenomena via flow simulations, we studied the effect of the type of 2D wrapping nanomaterial, catalyst and peroxide concentration upon micromotor speed. As shown in **Figure 3B**, speed increase along peroxide fuel concentrations from (5 to 10 %) from 13 ± 4 to 61 ± 30 µm/s (GO), 52 ± 36 to 108 ± 35 µm/s (GDY) and 14 ± 6 to 61 ± 29 µm/s (BP) when using Pt as catalyst. Interestingly, similar speeds were noted when using MnO_2 as trigger for micromotor propulsion. No apparent differences among micromotors using different 2D wrapping nanomaterials or catalyst are noted, probably due to the fact that catalyst are deposited over the exposed Au layer with the same surface roughness. Yet, in *bubble-magnetic* mode, clear differences can be seen among micromotors propelled by Pt or MnO_2 as a catalyst. Thus, after magnetic guidance the speed of Pt micromotors increase up to 75 % (in terms of speed increase, see **Figure 3C**, **b**) with a similar trend despite different 2D wrapping nanomaterials or peroxide levels are used. On the contrary, a lower speed increase percentage (40-50 %) is noted in MnO_2 micromotors in magnetic mode, with the effect more pronounced at low peroxide levels. Few studies can be found in the literature about the hydrodynamics related with the motion of bubble-propelled Janus micromotors. An early model suggested that the mechanism of bubble propulsion is due to the thrust produced by bubble disengagement,[53] similar to tubular micromotors. Yet, a more recent study found that the previous models do not fits well with Janus micromotors (due to shape changes), attributing the fast bubble propulsion to the microbubble cavitation-induced jet flow. To further support such phenomena and observations, we selected different videos of the propulsion of the micromotors at 5 % peroxide levels and performed flow simulation to study the energy mapping of the fluid around the micromotors. For this simulation we measured the speed and direction of the micromotors, decomposing the speed (velocity, v) s v_x and v_y and defining a rotation frequency as RPM. Once all the parameters were set, the flow speed around the motor was measured. The simulation was performed using the Flow Simulation Computational Fluid Dynamics (CFD) tool within the Solidworks 3D CAD software. Fluid velocity in the horizontal plane was depicted for clarity showing a different fluid distribution profile upon the action of the micromotor both guided, and unguided. According to recent models, bubble-growth process in Janus colloids is driven by catalytic mechanisms, the bubble-growth process can be described by the Rayleigh–Plesset equation (physical cavitation mechanism).[54] Yet, according to recent studies and to microbubble cavitation-induced jet flow, bubble evolution and ejection is not the sole mechanism responsible for micromotor propulsion.[55-58] Thus, another key issue needing clarification is the origin of fast, instantaneous propulsion after bubble collapse, so it is important to study the influence of the flow field to further explaining the dynamics. Considering that the bubble and the micromotors usually do not locate in the same horizontal plane due to the difference of their density, the jet flow is not strictly in the horizontal plane. In other words, the main source of the fast bubble propulsion on both modes is the horizontal component of the micromotor produced by the bubble collapse rather than the impulse when the bubble leaves the surface of the Janus micromotor. As can be seen in the simulation images of **Figure 3D**, a higher energy (in terms of velocity) is observed around the Janus micromotors in *bubble-magnetic* mode. According to the bubble cavitation-induced mechanism, this indicate a better distribution of the energy propelling the micromotor, which therefore can significantly improve the propulsion efficiency. Thus, it can be concluded that the orientation of the micromotor trajectory in *bubble-magnetic* mode (in comparison to *bubble-mode*) allow for a better distribution of the propelling energy of the micromotor, resulting in higher speeds. In other words, the increase of the directionality of the micromotor by orientation with the magnetic field can also contribute to such speed enhancement due to better fuel contact with the active nanoparticles, similar to a previous model described by our research group for tubular micromotors, which demonstrate that orienting the micromotors generates a speed increase due to the better fuel availability in the inner catalytic part.[59] The difference between the catalysts (Pt or MnO_2) can arise from its different ability to distribute such energy or to a different loading of Fe_2O_3 magnetic engines.[54, 60] Next, for future practical applications of the micromotors, we characterized its propulsion in real samples (saliva, milk, blood serum and wine). As the magnetic effect is more pronounced for Pt micromotors, we chose them for this study. As can be seen in **Figure S1 and Video S6** of the supporting information, despite the high viscosity and complexity of the media, micromotors propels at similar speeds to that observed in water samples in bubble mode. Yet, in *bubble-magnetic* mode the speed increase effect is similar for wine samples, with a slight decrease in more viscous, high-protein content saliva, milk and blood serum samples, probably due to the high viscosity of the samples disturb somehow the improved energy distribution along the micromotors. On overall, the high towing force of the dual propelled (*bubble-magnetic*) microengines hold considerable promise for applications in complex samples, which are prevented by hampered locomotion.

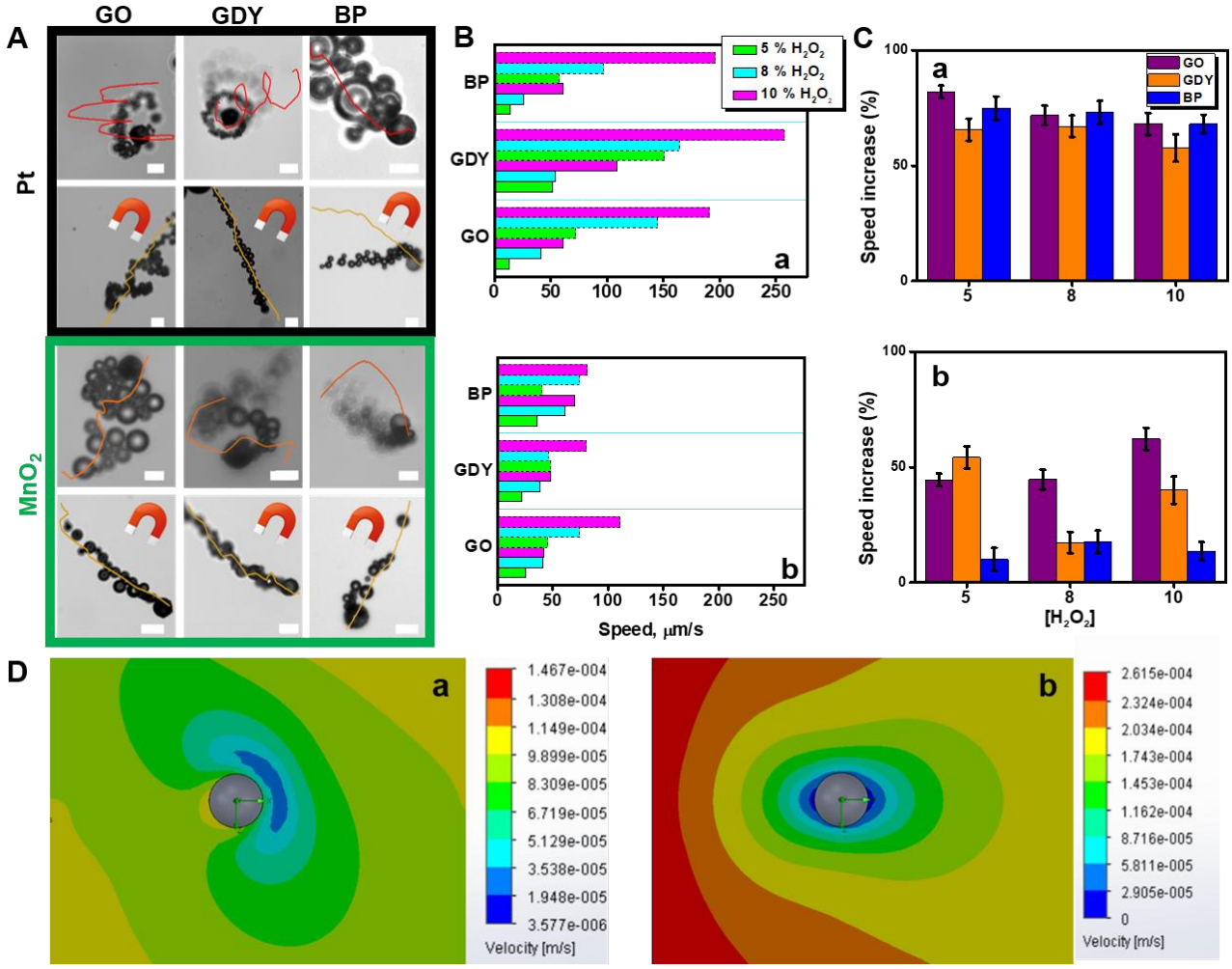

Figure 3. *Bubble-magnetic* hybrid Janus micromotor propulsion. A) Time-lapse images (Taken from **Videos S2 and S3**) showing the propulsion and corresponding tracking lines (over 2s period) of the micromotors in *bubble* and *bubble-magnetic* mode. B) Influence of the nanomaterial (GO, GDY and BP), catalyst (a Pt and b MnO_2) and hydrogen peroxide concentration upon the micromotor speed in both *bubble* (continuous line in the graph bar) and *bubble-magnetic* (dotted line in the graph bar) modes. C) Graph showing the speed increase (a Pt micromotors and b MnO_2 micromotors) after switching from *bubble-mode* to *bubble-magnetic mode*. D) Simulated flow and energy mapping around the Janus micromotors structure in *bubble* (a) and *bubble-magnetic* (b) modes (see also **Videos S4 and S5**). Scale bar, 20 μm.

In another conceptual step ahead, the *bubble-magnetic-light "three way"* hybrid micromotor propulsion was also explored (see **Figure 4**). As previously described, micromotors contain CdSe@ZnS QDs as "*third engine handle*" for acceleration-braking by light irradiation. The mechanism is depicted in **Figure 4A**. Upon UV or visible light irradiation, the QDs used as engine in the micromotor surface absorb photons with energies equal or higher than its bandgap energy (2.4 eV); promoting the migration of the electrons present in the valence band to the conduction band. The 2D nanomaterial layer can act as electron acceptor, promoting electron transfer towards the asymmetric Pt/Fe_2O_3 or MnO_2/Fe_2O_3 layers.[61] In the case of Pt, electrons accumulate in such layer resulting in a negative net charge that reacts with oxygen and protons present in the media, generating an additional peroxide fuel input which is further decomposed to increase the micromotor speed. In the case of MnO_2, its inherent photocatalytic behavior results in the pairing of the releasing electrons with its electronic levels and subsequent promotion to the conduction band. This generates holes (h^+) which also react with the peroxide fuel to release additional O_2 bubbles for the micromotor acceleration.[28] As in the previous case, we studied the effect of the type of 2D wrapping nanomaterial and catalyst upon micromotor speed. Light intensity effect was also evaluated. The combined effect of light, wrapping nanomaterials and catalyst is shown in the time lapse-images of **Figure4B**. Once the micromotors were propelling by *bubble-mode* at a fixed 5% peroxide level, different light illuminations were used to activate the light engine of each motor by promoting electron release from the QDs. Such light corresponds to variable photon energies: 385 nm (3.2 eV), 470 nm (2.6 eV) and 550 nm (2.3 eV). Thus, after light irradiation (see **Figure S2** in the Supporting Information) the initial speed of the micromotors in *bubble-mode* increase from 39 ± 21 to 44 ± 15 μm/s and 75 ± 12 μm/s after exposure to UV (385 nm) and blue (470 nm) light when using Pt. This corresponds to a speed increase of over 10 to 15 % and 30 %, respectively. A similar trend was observed regarding the wrapping 2D nanomaterials, whereas the speeds depend greatly on the light used. It should be mentioned here that at 550 nm no apparent speed increase is noted due to the band gap (2.3 eV) is lower than the band gap of the QDs (2.4 eV), preventing thus electron promotion. In the case of MnO_2 micromotors (and regarding the effect of the catalyst) speed increase from 26 ± 12

to 42 ± 15 µm/s and 48 ± 12 µm/s after exposure to UV (385 nm) and blue (470 nm) light. This corresponds to speed increase of over 50 % (in terms of speed increase, see **Figure 4C**, **b**), which is higher than that for Pt engines, probably due to more efficient electron promotion and products generation. As for Pt engines, no apparent acceleration is noted at 550 nm. In addition, no influence of the 2D nanomaterial is noted. Thus, it can be concluded that main variables to control the braking/acceleration system in bubble-light mode were light intensity (wavelength) and catalyst (Pt or MnO_2).

After characterizing the motion in *bubble-light* mode, we applied the magnetic field to activate the magnetic engine and record the resulting speed. For Pt microengines, speed increase in all cases is within the same magnitude to that noted in *bubble-magnetic mode*, indicating that the towing force of the magnetic activated engine surpasses the light engine (**Figure 4C**, a, dotted line). On the contrary, for MnO_2 microengines, a much great speed increase of up to 60 % (GO), 73 % (GDY) and 34 % (BP) is noted, which is from 1.4 to 3.4 times higher than *bubble-magnetic* mode, indicating the additive effect of both improved light induced oxygen generation and magnetic enhanced energy distribution (**Figure 4C**, b, dotted line). Additionaly, to check a possible effect of Fe_2O_3 NPs on the light motion, we performed the light only experiments with QDs-modified micromotors without the addition of the magnetic nanoparticles. No apparent speed increase is observed, revealing the negligible contribution of such magnetic nanoparticles. Also, in the UV-VIS images of micromotors containing Fe_2O_3 and PtNPs nanoparticles (bare micromotors, **Figure 2C**) no apparent adsorption bands are noted, as compared with micromotors containing QDs, further supporting the above-mentioned observation. Additional 3D flow numerical simulations to study the energy mapping of the fluid around the micromotors illustrate a similar trend in *bubble* and *bubble-light* modes, with a slight increase in the velocity (energy) due to the enhanced fuel or oxygen generation (see **Figure 4D**). For bubble-light-magnetic mode, the distribution is like that of *bubble-magnetic* mode. Thus, it can be concluded that main variables to control the braking/acceleration system in *bubble-light-magnetic* mode were also light intensity (wavelength) and catalyst (Pt or MnO_2).

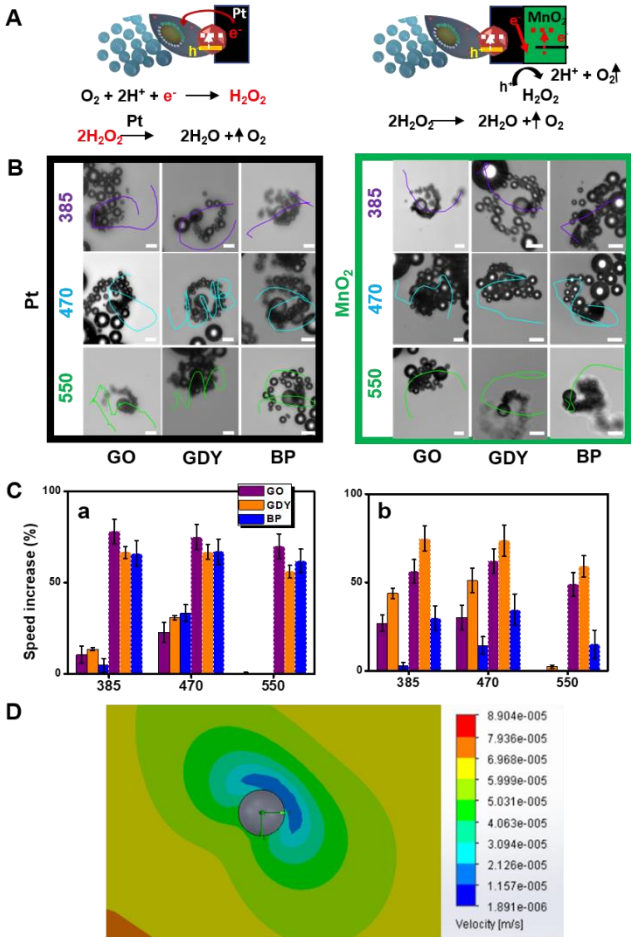

Figure 4. *Bubble-light-magnetic* hybrid Janus micromotor propulsion. A) Schematic of the mechanism responsible for *bubble-light-magnetic* Janus micromotor propulsion. B) Influence of the nanomaterial (GO, GDY and BP), catalyst and light wavelength upon the micromotor speed in *bubble-light* mode: time-lapse images (Taken from **Videos S7 and S8**) showing the propulsion and corresponding tracking lines (over 2s period) of the micromotors in *bubble* and *bubble-light* mode. C) Graph showing the speed increase (a Pt and b MnO_2) experience after switching from *bubble-light* (continuous line in the graph bar) mode to *bubble-light-magnetic* (dotted line in the graph bar) mode. D) Simulated flow and turbulent energy mapping around the Janus micromotors structure in *bubble-light* (a) and *bubble-light magnetic* mode (b) (see **Video S9 and Video S10**). Scale bars, 20 µm.

Next, for future practical applications of the micromotors, we characterized its propulsion in real samples (saliva, milk, blood serum and wine). As can be seen in **Figure S3 and Video S11** of the supporting information, despite the high viscosity and complexity of the media, the combined effect of *bubble-light and magnetic* fields leads to a highly remarkable speed in all the samples tested despite the high complexity in some cases. Such speeds are higher (from 1.5 to 2 times) when compared to the similar study performed in *bubble-magnetic* mode, reflecting the superior capabilities of the combination of the three systems in a single engine.

CONCLUSIONS

In conclusion, we have described the preparation of multi-stimulate driven Janus micromotors with *built-in* engines for

bubble, magnetic, light driven propulsion and hybrid schemes. For the first time, the micromotor body also incorporate not only well-established 2D nanomaterials (GO) but novel ones (GDY and BP) with rich outer surface chemistry to be exploited in future applications. Different variables such as type of engines (Pt or MnO_2 nanoparticles), peroxide fuel and light can be modulated to tailor the micromotor propulsion in each mode. Thus, in *bubble mode* speed modulation can be achieved by changing the fuel composition, as in common catalytic micromotors. Surprisingly, in *bubble-magnetic* mode main variables were peroxide level and type of catalyst used, with a speed increase of up to 75 % (in terms of speed increase) for Pt based microengines and up to 50 % for MnO_2 micromotors in magnetic mode, with the effect more pronounced at low peroxide levels. In *bubble-light* mode, the braking-acceleration system can be tailored by modulating light intensity (wavelength) and catalyst (Pt or MnO_2), with a change in the speed increase trend of 50 % for MnO_2 and 30 % for PtNPs, probably due to a better synergetic effect between CdSe@ZnS QDs to promote electron transfer. Finally, in *bubble-light-magnetic* mode, when using PtNPs the effect of magnetic fields surpasses the light-enhanced acceleration whereas a synergetic effect between the three engines is noted for MnO_2, with a speed increase of over 73 %. Numerical simulations illustrate that such adaptative behavior and improved propulsion efficient is produced by a better distribution of the energy propelling the micromotor by activation of the magnetic and/or light engines following the so-called bubble cavitation-induced mechanism. The new micromotors offer a myriad of controllable propulsion behaviors, which along the incorporation of functional nanomaterials such as BP or GDY, will serve to the rational and mass-scale design of hybrid microrobotics for a wide range of applications with unpreceded performance.

ASSOCIATED CONTENT

Supporting Information. This material is available free of charge via the Internet at http://pubs.acs.org

Supporting figures (pdf)

Multi-catalytic, light and magnetic propulsion of GDY-PtNPs-Fe_2O_3-QDs Janus micromotors in 5 % H_2O_2 (AVI)

Bubble-magnetic propulsion of 2D nanomaterials-PtNPs-Fe_2O_3-QDs Janus micromotors in 5 % H_2O_2 (AVI)

Bubble-magnetic propulsion of 2D nanomaterials-PtNPs-MnO_2-QDs Janus micromotors in 5 % H_2O_2 (AVI)

Simulated flow energy mapping around the micromotor in bubble mode (AVI)

Simulated flow energy mapping around the micromotor in bubble-magnetic mode (AVI)

Janus micromotors propulsion in real samples in bubble-magnetic mode (AVI)

Bubble-light propulsion of 2D nanomaterials-PtNPs-Fe_2O_3-QDs Janus micromotors in 5 % H_2O_2 (AVI)

Bubble-light propulsion of 2D nanomaterials-MnO_2-Fe_2O_3-QDs Janus micromotors in 5 % H_2O_2 (AVI)

Simulated flow energy mapping around the micromotor in bubble-light mode (AVI)

Simulated flow energy mapping around the micromotor in bubble-light-magnetic mode (AVI)

Janus micromotors propulsion in real samples in bubble-magnetic-light mode (AVI)

AUTHOR INFORMATION

Corresponding Author

* alberto.escarpa@uah.es

* beatriz.jurado@uah.es

Author Contributions

The manuscript was written through contributions of all authors. All authors have given approval to the final version of the manuscript.

Notes

The authors declare no competing financial interest.

ACKNOWLEDGMENT

K. Yuan acknowledges the Spanish Ministry of Science, Innovation and Universities for his pre-doctoral contract (RYC-2015-17558, co-financed by EU). V. de la Asunción-Nadal acknowledges the FPI fellowship received from the University of Alcala. B. J-S acknowledges support from the Spanish Ministry of Science, Innovation and Universities (RYC-2015-17558, co-financed by EU) from the University of Alcala (CCG19/CC-029) and from the UAH/Community of Madrid (CM/JIN/2019-007). AE acknowledges financial support from the Spanish Ministry of Science, Innovation and Universities (CTQ2017-86441-C2-1-R) and the TRANSNANOAVANSENS program (S2018/NMT-4349) from the Community of Madrid.

REFERENCES

1. Paxton, W. F.; Kistler, K. C.; Olmeda, C. C.; Sen, A.; St. Angelo, S. K.; Cao, Y.; Mallouk, T. E.; Lammert, P. E.; Crespi, V. H., Catalytic Nanomotors: Autonomous Movement of Striped Nanorods. *J. Am. Chem. Soc.* **2004,** 126, 13424-13431.

2. Kline, T. R.; Paxton, W. F.; Sen, A., Catalytic Nanomotors: Remote-Controlled Autonomous Movement of Striped Metallic Nanorods. *Angew. Chem. Int. Ed.* **2005,** 117, 754-756.

3. Paxton, W. F.; Sundararajan, S.; Mallouk, T. E.; Sen, A., Chemical Locomotion. *Angew. Chem. Int. Ed.* **2006,** 45, 5420-5429.

4. Gao, W.; Sattayasamitsathit, S.; Orozco, J.; Wang, J., Highly Efficient Catalytic Microengines: Template Electrosynthesis of Polyaniline/Platinum Microtubes. *J. Am. Chem. Soc.* **2011,** 133, 11862-11864.

5. Gao, W.; Sattayasamitsathit, S.; Uygun, A.; Pei, A.; Ponedal, A.; Wang, J., Polymer-based tubular microbots: role of composition and preparation. *Nanoscale* **2012,** 4, 2447-2453.

6. Wang, W.; Castro, L. A.; Hoyos, M.; Mallouk, T. E., Autonomous Motion of Metallic Microrods Propelled by Ultrasound. *ACS Nano* **2012,** 6, 6122-6132.

7. Garcia-Gradilla, V.; Orozco, J.; Sattayasamitsathit, S.; Soto, F.; Kuralay, F.; Pourazary, A.; Katzenberg, A.; Gao, W.; Shen, Y.; Wang, J., Functionalized Ultrasound-Propelled Magnetically Guided Nanomotors: Toward Practical Biomedical Applications. *ACS Nano* **2013,** 7, 9232-9240.

8. Wang, J., *Nanomachines: Fundamentals and Applications* **2013**. Wiley VCH.

9. Chen, X.-Z.; Hoop, M.; Mushtaq, F.; Siringil, E.; Hu, C.; Nelson, B. J.; Pané, S., Recent developments in magnetically driven micro- and nanorobots. *Appl. Mater. Tod.* **2017,** 9, 37-48.

10. Karshalev, E.; Esteban-Fernández de Ávila, B.; Wang, J., Micromotors for "Chemistry-on-the-Fly". *J. Am. Chem. Soc.* **2018,** 140, 3810-3820.

11. Ren, L.; Wang, W.; Mallouk, T. E., Two Forces Are Better than One: Combining Chemical and Acoustic Propulsion for Enhanced Micromotor Functionality. *Acc. Chem. Res.* **2018,** 51, 1948-1956.
12. Chen, C.; Soto, F.; Karshalev, E.; Li, J.; Wang, J., Hybrid Nanovehicles: One Machine, Two Engines. *Adv. Funct. Mater.* **2019,** 29, 1806290.
13. Wang, C.; Dong, R.; Wang, Q.; Zhang, C.; She, X.; Wang, J.; Cai, Y., One Modification, Two Functions: Single Ni-modified Light-Driven Microrockets with Both Efficient Propulsion and Steerable Motion. *Chem. Asian J.* **2019**, 14, 2485-2490.
14. Wang, D.; Zhao, G.; Chen, C.; Zhang, H.; Duan, R.; Zhang, D.; Li, M.; Dong, B., One-Step Fabrication of Dual Optically/Magnetically Modulated Walnut-like Micromotor. *Langmuir* **2019,** 35, 2801-2807.
15. Gao, W.; Manesh, K. M.; Hua, J.; Sattayasamitsathit, S.; Wang, J., Hybrid Nanomotor: A Catalytically/Magnetically Powered Adaptive Nanowire Swimmer. *Small* **2011,** 7, 2047-2051.
16. Jurado-Sánchez, B.; Pacheco, M.; Rojo, J.; Escarpa, A., Magnetocatalytic Graphene Quantum Dots Janus Micromotors for Bacterial Endotoxin Detection. *Angew. Chem. Int. Ed*. **2017,** 56, 6957-6961.
17. Li, J.; Li, T.; Xu, T.; Kiristi, M.; Liu, W.; Wu, Z.; Wang, J., Magneto–Acoustic Hybrid Nanomotor. *Nano Lett.* **2015,** 15, 4814-4821.
18. Ren, L.; Zhou, D.; Mao, Z.; Xu, P.; Huang, T. J.; Mallouk, T. E., Rheotaxis of Bimetallic Micromotors Driven by Chemical–Acoustic Hybrid Power. *ACS Nano* **2017,** 11, 10591-10598.
19. Xu, T.; Soto, F.; Gao, W.; Dong, R.; Garcia-Gradilla, V.; Magaña, E.; Zhang, X.; Wang, J., Reversible Swarming and Separation of Self-Propelled Chemically Powered Nanomotors under Acoustic Fields. *J. Am. Chem. Soc.* **2015,** 137, 2163-2166.
20. Xu, T.; Soto, F.; Gao, W.; Garcia-Gradilla, V.; Li, J.; Zhang, X.; Wang, J., Ultrasound-Modulated Bubble Propulsion of Chemically Powered Microengines. *J. Am. Chem. Soc.* **2014,** 136, 8552-8555.
21. Jang, B.; Wang, W.; Wiget, S.; Petruska, A. J.; Chen, X.; Hu, C.; Hong, A.; Folio, D.; Ferreira, A.; Pané, S.; Nelson, B. J., Catalytic Locomotion of Core–Shell Nanowire Motors. *ACS Nano* **2016,** *10*, 9983-9991.
22. Tang, S.; Zhang, F.; Zhao, J.; Talaat, W.; Soto, F.; Karshalev, E.; Chen, C.; Hu, Z.; Lu, X.; Li, J.; Lin, Z.; Dong, H.; Zhang, X.; Nourhani, A.; Wang, J., Structure-Dependent Optical Modulation of Propulsion and Collective Behavior of Acoustic/Light-Driven Hybrid Microbowls. *Adv. Funct. Mater.* **2019**, 29, 1809003.
23. Xing, Y.; Zhou, M.; Du, X.; Li, X.; Li, J.; Xu, T.; Zhang, X., Hollow Mesoporous Carbon@Pt Janus Nanomotors with Dual Response of H_2O_2 and Near-Infrared Light for Active Cargo Delivery. *Appl Mater Tod* **2019,** *17*, 85-91.
24. Villa, K.; Novotný, F.; Zelenka, J.; Browne, M. P.; Ruml, T.; Pumera, M., Visible-Light-Driven Single-Component $BiVO_4$ Micromotors with the Autonomous Ability for Capturing Microorganisms. *ACS Nano* **2019,** *13*, 8135-8145.
25. Villa, K.; Pumera, M., Fuel-free light-driven micro/nanomachines: artificial active matter mimicking nature. *Chem. Soc. Rev.* **2019**, *48*, 4966-4978.
26. Chen, C.; Tang, S.; Teymourian, H.; Karshalev, E.; Zhang, F.; Li, J.; Mou, F.; Liang, Y.; Guan, J.; Wang, J., Chemical/Light-Powered Hybrid Micromotors with "On-the-Fly" Optical Brakes. *Angew. Chem. Int. Ed*. **2018,** 57, 8110-8114.
27. Jang, B.; Hong, A.; Kang, H. E.; Alcantara, C.; Charreyron, S.; Mushtaq, F.; Pellicer, E.; Büchel, R.; Sort, J.; Lee, S. S.; Nelson, B. J.; Pané, S., Multiwavelength Light-Responsive Au/B-TiO_2 Janus Micromotors. *ACS Nano* **2017,** *11*, 6146-6154.
28. María Hormigos, R.; Jurado-Sánchez, B.; Escarpa, A., Multi-Light-Responsive Quantum Dot Sensitized Hybrid Micromotors with Dual-Mode Propulsion. *Angew. Chem. Int. Ed*. **2019,** 58, 3128-3132.
29. Dong, R.; Wang, C.; Wang, Q.; Pei, A.; She, X.; Zhang, Y.; Cai, Y., ZnO-based Microrockets with Light-enhanced Propulsion. *Nanoscale* **2017,** 9, 15027-15032.
30. Maria-Hormigos, R.; Jurado-Sánchez, B.; Vazquez, L.; Escarpa, A., Carbon Allotrope Nanomaterials Based Catalytic Micromotors. *Chem. Mater.* **2016,** 28, 8962-8970.
31. Martín, A.; Jurado-Sánchez, B.; Escarpa, A.; Wang, J., Template Electrosynthesis of High-Performance Graphene Microengines. *Small* **2015,** 11, 3568-3574.
32. Ye, H.; Kang, J.; Ma, G.; Sun, H.; Wang, S., High-speed Graphene@Ag-MnO_2 Micromotors at Low Peroxide Levels. *J. Coll. Interfac. Sci.* **2018,** 528, 271-280.
33. Vilela, D.; Parmar, J.; Zeng, Y.; Zhao, Y.; Sánchez, S., Graphene-Based Microbots for Toxic Heavy Metal Removal and Recovery from Water. *Nano Lett.* **2016,** 16, 2860-2866.
34. Ma, X.; Katuri, J.; Zeng, Y.; Zhao, Y.; Sanchez, S., Surface Conductive Graphene-Wrapped Micromotors Exhibiting Enhanced Motion. *Small* **2015,** 11, 5023-5027.
35. Maric, T.; Moo, J. G. S.; Khezri, B.; Sofer, Z.; Pumera, M., Black-Phosphorus-enhanced Bubble-propelled Autonomous Catalytic Microjets. *Appl. Mater. Tod*. **2017,** 9, 289-291.
36. Singh, V. V.; Kaufmann, K.; Esteban Fernández de Ávila, B.; Karshalev, E.; Wang, J., Molybdenum Disulfide-Based Tubular Microengines: Toward Biomedical Applications. *Adv. Funct. Mater.* **2016,** 26, 6270-6278.
37. Mayorga-Martinez, C. C.; Moo, J. G. S.; Khezri, B.; Song, P.; Fisher, A. C.; Sofer, Z.; Pumera, M., Self-Propelled Supercapacitors for On-Demand Circuit Configuration Based on WS_2 Nanoparticles Micromachines. *Adv. Funct. Mater.* **2016,** *26*, 6662-6667.
38. Pourrahimi, A. M.; Villa, K.; Manzanares Palenzuela, C. L.; Ying, Y.; Sofer, Z.; Pumera, M., Catalytic and Light-Driven ZnO/Pt Janus Nano/Micromotors: Switching of Motion Mechanism via Interface Roughness and Defect Tailoring at the Nanoscale. *Adv. Funct. Mater.* **2019**, 29, 1808678.
39. Jia, Z.; Li, Y.; Zuo, Z.; Liu, H.; Huang, C.; Li, Y., Synthesis and Properties of 2D Carbon-Graphdyine. *Acc. Chem. Res.* **2017,** 50, 2470-2478.
40. Qi, H.; Yu, P.; Wang, Y.; Han, G.; Liu, H.; Yi, Y.; Li, Y.; Mao, L., Graphdiyne Oxides as Excellent Substrate for Electroless Deposition of Pd Clusters with High Catalytic Activity. *J. Am. Chem. Soc.* **2015,** 137, 5260-5263.
41. Kang, J.; Wells, S. A.; Wood, J. D.; Lee, J.-H.; Liu, X.; Ryder, C. R.; Zhu, J.; Guest, J. R.; Husko, C. A.; Hersam, M. C., Stable Aqueous Dispersions of Optically and Electronically Active Phosphorene. *Proc. Natl. Ac. Sci.* **2016,** 113, 11688-11693.
42. Liu, Y.; Wang, Y.; Ikram, M.; Lv, H.; Chang, J.; Li, Z.; Ma, L.; Rehman, A. U.; Lu, G.; Chen, J.; Shi, K., Facile Synthesis of Highly Dispersed Co_3O_4 Nanoparticles on Expanded, Thin Black Phosphorus for a ppb-Level NOx Gas Sensor. *ACS Sens.* **2018,** 3, 1576-1583.
43. Zhao, Y.; Zhou, Y.; O'Hayre, R.; Shao, Z., Electrocatalytic Oxidation of Methanol on Pt Catalyst Supported on Nitrogen-doped Graphene Induced by Hydrazine Reduction. *J. Phys. Chem. Solids* **2013,** 74, 1608-1614.
44. Wu, S.; Chen, W.; Yan, L., Fabrication of a 3D MnO_2/graphene Hydrogel for High-Performance Asymmetric Supercapacitors. *J. Mater. Chem. A* **2014,** 2, 2765-2772
45. Pawar, A. B.; Kretzschmar, I., Fabrication, Assembly, and Application of Patchy Particles. *Macromol. Rapid Commun*. **2010,** 31, 150-168.
46. Pacheco, M.; Jurado-Sánchez, B.; Escarpa, A., Lab-on-a-Micromotor: Catalytic Janus Particles as Mobile Microreactors for Tailored Synthesis of Nanoparticles. *Chem. Sci.* **2018,** 9, 8056-8064.
47. Straney, P. J.; Marbella, L. E.; Andolina, C. M.; Nuhfer, N. T.; Millstone, J. E., Decoupling Mechanisms of Platinum Deposition on Colloidal Gold Nanoparticle Substrates. *J. Am. Chem. Soc.* **2014,** 136, 7873-7876.
48. Fan, F.-R.; Liu, D.-Y.; Wu, Y.-F.; Duan, S.; Xie, Z.-X.; Jiang, Z.-Y.; Tian, Z.-Q., Epitaxial Growth of Heterogeneous Metal Nanocrystals: From Gold Nano-octahedra to Palladium and Silver Nanocubes. *J. Am. Chem. Soc.* **2008,** 130, 6949-6951.
49. Gu, D.; Tseng, J.-C.; Weidenthaler, C.; Bongard, H.-J.; Spliethoff, B.; Schmidt, W.; Soulimani, F.; Weckhuysen, B. M.; Schüth, F., Gold on Different Manganese Oxides: Ultra-Low-Temperature CO Oxidation over Colloidal Gold Supported on Bulk-MnO_2 Nanomaterials. *J. Am. Chem. Soc.* **2016,** 138, 9572-9580.
50. Zhang, M.; Wang, X.; Sun, H.; Wang, N.; Lv, Q.; Cui, W.; Long, Y.; Huang, C., Enhanced Paramagnetism of Mesoscopic Graphdiyne by Doping with Nitrogen. *Sci. Rep*. **2017,** 7, 11535.
51. Wu, J.-B.; Lin, M.-L.; Cong, X.; Liu, H.-N.; Tan, P.-H., Raman Spectroscopy of Graphene-based Materials and its Applications in Related Devices. *Chem. Soc. Rev.* **2018,** 47, 1822-1873.

52. Aldave, S. H.; Yogeesh, M. N.; Zhu, W.; Kim, J.; Sonde, S. S.; Nayak, A. P.; Akinwande, D., Characterization and Sonochemical Synthesis of Black phosphorus from Red Phosphorus. *2D Mater.* **2016,** 3, 014007.
53. Li, L.; Wang, J.; Li, T.; Song, W.; Zhang, G., A Unified Model of Drag Force for Bubble-propelled Catalytic Micro/nano-motors with Different Geometries in Low Reynolds Number Flows. *J. Appl. Phys.* **2015,** 117, 104308.
54. Zhang, J.; Zheng, X.; Cui, H.; Silber-Li, Z., The Self-Propulsion of the Spherical Pt–SiO_2 Janus Micro-Motor. *Micromachines* **2017,** 8, 123.
55. Manjare, M.; Yang, B.; Zhao, Y. P., Bubble Driven Quasioscillatory Translational Motion of Catalytic Micromotors. *Phys. Rev. lett.* **2012,** 109, 128305.
56. Zwaan, E.; Le Gac, S.; Tsuji, K.; Ohl, C.-D., Controlled Cavitation in Microfluidic Systems. *Phys. Rev. Lett.* **2007,** 98, 254501.
57. Michelin, S.; Lauga, E., Geometric Tuning of Self-Propulsion for Janus Catalytic Particles. *Sci. Rep*. **2017,** 7, 42264.
58. Yang, F.; Manjare, M.; Zhao, Y.; Qiao, R., On the Peculiar Bubble Formation, Growth, and Collapse Behaviors in Catalytic Micro-motor Systems. *Microfluid. Nanofluid*. **2017,** 21, 6.
59. de la Asunción-Nadal, V.; Jurado-Sánchez, B.; Vázquez, L.; Escarpa, A., Magnetic Fields Enhanced the Performance of Tubular Dichalcogenide Micromotors at Low Hydrogen Peroxide Levels. *Chem. Eur. J.* **2019,** *25*, 13157-13163.
60. Wang, L. L.; Chen, L.; Zhang, J.; Duan, J. M.; Wang, L.; Silber-Li, Z. H.; Zheng, X.; Cui, H. H., Efficient Propulsion and Hovering of Bubble-Driven Hollow Micromotors underneath an Air-Liquid Interface. *Langmuir* **2018,** 34, 10426-10433.
61. Wang, M.; Shang, X.; Yu, X.; Liu, R.; Xie, Y.; Zhao, H.; Cao, H.; Zhang, G., Graphene–CdS Quantum Dots–Polyoxometalate Composite Films for Efficient Photoelectrochemical Water Splitting and Pollutant Degradation. *Phys. Chem. Chem. Phys.* **2014,** 16, 26016-26023.

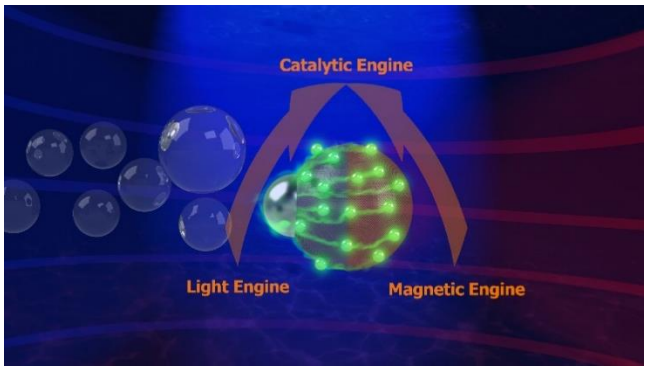
Catalytic Engine
Light Engine
Magnetic Engine